



Vibration Transmission of Ballastless Track-bridge with Different Span Lengths under Updated High-speed Trains

Rui Zhou^{1d,a,c,e}, Fuyan Yang^a, Hanlin Liu^{1b,c}, Jingmang Xu^c, Qingsong Feng^d, and Shiya Li^e

^aCollege of Civil and Transportation Engineering, Shenzhen University, Shenzhen 518060, China

^bMining College, Guizhou University, Guizhou 550025, China

^cMOE Key Laboratory of High-Speed, Railway Engineering, Southwest Jiaotong University, Chengdu 610031, China

^dState Key Laboratory of Performance Monitoring and Protecting of Rail Transit Infrastructure, East China Jiaotong University, Nanchang 330044, China

^eState Key Laboratory of Mountain Bridge and Tunnel Engineering, Chongqing Jiaotong University University, Chongqing 400074, China

ARTICLE HISTORY

Received 17 November 2023
Revised 4 March 2024
Accepted 16 April 2024
Published Online 4 July 2024

KEYWORDS

Updated train speeds
Vehicle-ballastless track-bridge structure
Rigid-flexible coupling model
Vibration transmission
Safety evaluation

ABSTRACT

As an important indicator of dynamic performance, the vibration transmission among multi-layer track-bridge structures for different bridge spans under the updated 400 km/h train loads are not clear. The vibration transmissions of the longitudinal slab track-bridge on three typical bridge span lengths (i.e., 24 m, 32 m, and 40 m) under five updated train speeds and three train weights were investigated in this paper by developing a refined vehicle-track-bridge model. The results show that the wheel load reduction rate, acceleration, and contact force gradually increase as train speed and train load increase, especial for the vertical vibration of 40 m span. The lateral displacement of the track structure on the 32 m span and the vertical displacement of the track structure on the 40m span are the largest among three spans. The vertical vibration transmission at 200 km/h is the highest among five train speeds, and the acceleration transmission of the 24 m span is larger than that of two other spans before 300 km/h. The vertical wheel-rail contact forces of the 40 m span under 100% capacity are close to the allowable limit values, and all of current track-bridge structures could meet the needs of the 400 km/h speed.

1. Introduction

With the vigorous development of China's high-speed railways, 40 m span girder bridges is continuously extending to wider and more complex areas instead of the 32 m span due to the aviod of sympathetic vibration, and 400 km/h train speed and full train load will be gradually promoted and applied in the next generation of high-speed train. The bridge is widely used as a foundation to support the railway system result of its high stiffness and strength which lead to relatively small differential settlement (Yan et al., 2015; Montenegro et al., 2021; Zheng et al., 2022). For example, around 50% of the 41,000 km long high-speed railway is supported by simply-supported box girder bridges with four standard span lengths of 20 m, 24 m, 32 m, and 40 m, respectively. The bridge span length is related to the structural stiffness, which could significantly affect the vibration transmission and dynamic performance of the

Vehicle-Track-Bridge (VTB) coupling system (Zhai and Cai, 2002; Jeon et al., 2016; Gong et al., 2021; Yang et al., 2021; Zhu et al., 2024). In particular, the vibration transmission among multi-layer concrete components is an important indicator of dynamic performance for longitudinal slab track-bridge structure. With the continuously increase of the passenger carrying capacity and comfort requirement, the existing coupled vehicle-ballastless track-bridge structure could be subjected to increasing high speed and heavy train loading (i.e., up to 400 km/h and 30,000 tons) in the near future in China. With the continuously increase of train speed and weight, the relationship between the bridge span lengths, vibration transmission, and dynamic performance of different components in the coupling system is unclear. Therefore, the dynamic characteristic analysis of the longitudinal slab track-three bridge structures with various bridge spans under the updated higher train speed and heavier load should be further investigated.

CORRESPONDENCE Hanlin Liu ✉ liuhl@gzu.edu.cn Mining College, Guizhou University, Guizhou 550025, China; MOE Key Laboratory of High-Speed, Railway Engineering, Southwest Jiaotong University, Chengdu 610031, China

© 2024 Korean Society of Civil Engineers

A series of theoretical studies have been proposed to explore the numerical models of Vehicle-Track-Bridge (VTB) coupling system in high-speed railways, respectively. Xiang et al. (2021) used the software MIDAS/Civil to simulate the vehicle-track-continuous bridge model and found that the creep irregularity has a negative effect on the comfort of the moving train. As the dynamic performance of ballastless tracks under train loads, Chen et al. (2013) excited the single-wheel axle to measure the dynamic strain of slab tracks and analyzed the influence of the dynamic load magnification factor when the train speed increased. Gautier (2015) and Matias and Ferreira (2020) summarized the development of the dynamic characteristic of slab tracks under various train speeds from their first applications until today. It identified the potential advantages of the existing slab track systems subject to very high train speeds. Zhai et al. (2013a, 2013b, 2015a, 2015b) established the VTB coupling models with various speeds from 250 to 350 km/h to study their dynamic performance. However, the ballastless track in these numerical VTB models was assumed as a single-layer structure without considering the vibration transmission among multi-layer track-bridge structure under different train loads.

In addition, some researchers studied the dynamic performance in VTB structures with various bridge span lengths, including the 24 m, 32 m, and 40 m spans of the simply-supported bridge. Particularly, the effect differential in bridge stiffness needs to be analyzed under three bridge span lengths (i.e., 24 m, 32 m, and 40 m) on the vibration transmission of the coupled system. Chen (2020) proposed the methodology of evaluating longitudinally connected track subject to train load and long-term bridge deformation of 20 m, 24 m, and 32 m. Xia et al. (2012) used the 24 m span length of the vehicle-bridge coupled model to analyze the dynamic responses of railway bridges during a floating-ice

collision. By comparing with the bridges of 24 m and 32 m span, Chen et al. (2015) and Zhang et al. (2017) proposed the continuous beam and pier differential settlements in the various VTB coupled models and found that the wheel unloading and dynamic response in the 24 m slightly larger than a 32 m span length. Zhou et al. (2021) used the various stage fatigue loading test enrolling theory of deflection evolution and stiffness degradation to analyze the CRTS-II ballastless track-bridge structure with a 32 m span length. Based on a vehicle-bridge system with a bridge span of 40 m in the future, Li et al. (2013) analyzed the rayleigh damping parameters in the dynamic system. It shows the bridge displacement and vehicle acceleration decrease with the damping ratio increasing. Although much work has been done in this field, the dynamic performance of the existing vehicle-track-bridge system with various bridge span lengths under higher train speeds and weight has not been fully understood and further research is required.

Therefore, the paper targets to comprehensively explore the dynamic performance and vibration transmission of the ballastless track-bridge structures with three bridge spans under various future high-speed train conditions. Based on the commercial software package ANSYS and Universal Mechanism (UM) software, the train is numerically modeled as a multi-rigid body, the CRTS-II slab ballastless track is modeled as a multi-flexible body. Subsequently, the coupled VTB system was first validated using field measurement data. Parametric studies were then carried out to assess the dynamic characteristics of the track plate, base plate, and box girder under five train speeds and three train loads, respectively. It could precisely explore the dynamic performance of existing ballastless track-bridge structures under updated high-speed trains.

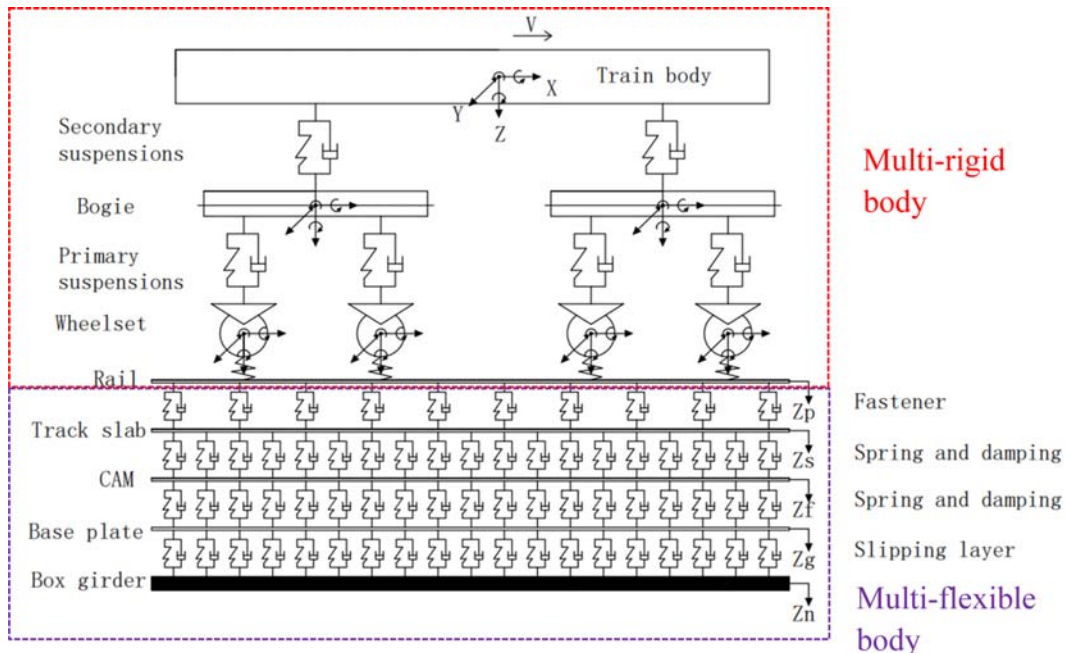


Fig. 1. The Coupled Vehicle-Ballastless Track-bridge Developed Model in This Study

2. Methods

2.1 Modeling the Coupled Vehicle-Track-Bridge (VTB) System

The developed model of the coupled vehicle-ballastless slab track-bridge system in this study is shown in Fig. 1. It shows that the coupled system includes a multi-rigid body and a multi-flexible body. Especially, the simulated multi-rigid body consists of a train body, two bogies, four wheelsets, and eight axle boxes with 15 rigid components. The primary spring suspension device is set to connect wheelsets and bogies, while the secondary spring suspension device is used to connect the train body and bogies. The multi-flexible body represents the CRTS II ballastless track-bridge structure which is modeled as a multi-layer structure consisting of rail, fasteners, track slab, Cement Asphalt Mortar (CAM) layer, base plate, slipping layer, and box girder in the vertical direction. The springs and damping are used to simulate layers' connection among the track slab, CAM layer, and base plate.

2.1.1 Modeling the High-Speed Train Using Multi-Rigid Body Dynamics

Assuming the model could ignore the train elastic deformation, there are 50 degrees of freedom in the train rigid model. The car body, wheelsets, and bogie have 6 degrees of freedom representing expansion, side rolling, lateral displacement, vertical displacement, head shaking, and nodding. In addition, the axle box is modeled as one degree of freedom representing vertical displacement. The interaction between different rigid bodies is modeled using spring and damping (Zhai, 2020). Thus, the governing equation describing the dynamic responses of multi-rigid body train system can be defined as,

$$\begin{cases} F(q, u, \dot{u}, \lambda, t) = 0 \\ G(u, q) = u - \dot{q} \\ \phi(q, t) = 0 \end{cases}, \quad (1)$$

where F is the differential equations of system mechanics, u is generalized velocity array, q is the generalized coordinate array, λ is the constraint force and action force array, G is the algebraic equations of generalized velocities, ϕ is the constrained algebraic equation array.

2.1.2 Modeling the Ballastless Track-bridge Structure Using Multi-Flexible-Body Dynamics

The CRTS-II ballastless track-bridge structure is modeled as a multi-layer structure consisting of rail, fasteners, track slab, CAM layer, base plate, slipping layer, and box girder in the vertical direction. The springs and damping are used to model the interaction between the track slab, CAM layer, base plate, and box girder. Based on the mode superposition method (Li et al., 2013), the ballastless track-bridge structure can be described as follows dynamic governing equation,

$$\begin{bmatrix} mI \ddot{d}_{CM} C_t \\ J \quad C_r \\ M_d \end{bmatrix} \begin{Bmatrix} a \\ \dot{\omega} \\ \ddot{q} \end{Bmatrix} + \begin{Bmatrix} m \tilde{\omega} \dot{d}_{CM} \\ \tilde{\omega} I \tilde{\omega} + G_r \omega \\ O_e \Omega + G_e \omega \end{Bmatrix} + \begin{Bmatrix} 0 \\ 0 \\ K_e q \end{Bmatrix} = \begin{Bmatrix} \sum_k P_k \\ \sum_k \tilde{C}_k P_k \\ \sum_k U^T(c_k) P_k \end{Bmatrix}, \quad (2)$$

where C_r , C_t are coupling matrix of translational and rotational deformation, M_e and J are modal mass matrix and moment of inertia, G_r , G_e are the turning force caused by rotation and deformation, O_e is the centrifugal force due to deformation, d_{CM} is the elastic displacement with respect to the center of gravity, a and ω are the absolute acceleration and angular acceleration. q is the modal coordinate and $\tilde{\omega}$ represents the vector product, $\tilde{\omega} = r \times \omega$.

2.1.3 Modelling the Coupled Rigid-Flexible Body System

Based on D'Alembert and the virtual work principle, all the constraint conditions are assumed to be ideal constraints, and the connections between the rigid and flexible bodies are modeled using the constraint conditions and force elements (Yang et al., 2021). The dynamic governing equations for the coupled rigid-flexible body system described as follows,

$$\begin{cases} M(q, t) \ddot{q} + \phi_q^T(q, t) \lambda = f(\dot{q}, q, t) \\ \phi(q, t) = 0 \end{cases}, \quad (3)$$

where $M(q, t) \in R^{n \times m}$ represent general mass, $q \in R^n$ is the system of global coordinate vector, $\lambda \in R^m$ is the Lagrange multiplier vector, $f(\dot{q}, q, t): R^n \times R^n \times R \rightarrow R^n$ represents the system of the general force vector, $\phi(q, t) = R^n \times R \rightarrow R^m$ is the Kinematic constraint equation, $\phi_q(q, t) = \partial \phi(q, t) / \partial q$ represents Jacobi matrix.

2.2 Numerical Solutions

2.2.1 Rigid Train Model

The CRH380 train is used for analysis in this study, the train mass and wheel mass are 40,460 and 1,869 kg, respectively. The axle box quality, static axial loading, and bogie structure quality are 50,11700,3338 kg, respectively (Ren et al., 2023). The primary suspension is modeled by a suspension spring and a shock absorber with vertical, lateral, and longitudinal stiffness of 1,040 kN/m, 4,000 kN/m, and 15,000 kN/m, respectively. As for the primary suspension, the vertical damping is set to 30 kN·s/m. The secondary suspension is composed of a secondary spring, secondary lateral damper, and anti-hunting damper with vertical stiffness is 400 kN/m, lateral is 240 kN/m, and longitudinal is 240 kN/m, respectively. The vertical damping of secondary suspension is 30 kN·s/m, lateral is 50 kN·s/m and longitudinal is 150 kN·s/m, respectively. Fig. 2 shows the force element function of assembling the whole train in UM software. Additionally, the secondary suspension of the bogie is connected through the use of force elements.

2.2.2 Flexible Model of Ballastless Track-Bridge Structure

Table 1 presents the parameters of the CRTS-II slab ballastless

Table 1. The Parameters of CRTS II Slab Ballastless Track Used in This Study

Parameter	Value	Unit
Elastic Modulus of rail	2.06×10^{11}	Pa
moment of inertia of the cross section of the rail	3.217×10^{-5}	M^4
Mass per unit length of rail	60.64	Kg/m
Dimension of track slab	$6450 \times 2550 \times 200$	mm
Elastic Modulus of track slab	3.3×10^{10}	N/m^2
Density of track slab	2500	kg/m^3
Dimension of CAM layer	$6450 \times 2,550 \times 30$	mm
Elastic Modulus of CAM layer	8.5×10^9	Pa
Density of CAM layer	2400	kg
Dimension of base plate	$6450 \times 2950 \times 200$	mm
Elastic Modulus of base plate	3×10^{10}	Pa
Density of base plate	2500	kg/m^3

track, which were determined using the ANSYS commercial Finite Element (FE) package. Fig. 2 depict the CRTS-II track, which has been modeled as a multi-layer structure with the CAM layer and base plate being represented using solid elements. The friction unit is introduced to model the layer that allows sliding between the base plate and the box girder incorporates geotextiles and the friction coefficient is assumed to be 0.3 (Zhou et al., 2022).

As shown in Fig. 2, two lines of CRTS-II tracks are supported by a prestressed C55 concrete box girder with simply-supported conditions in three different span lengths (i.e., 24 m, 32 m, and 40 m). For the box girder with a span of 24 m and 32 m, the width and height of the cross-section of the box girder are 12 m and 3.059 m, respectively. For the girder with a span of 40 m, the width and height of the cross-section are 12.6 m and 3.235m, respectively. The solid elements are used in the FE analysis with a total of 35880, 47840, and 67000 elements for the bridge with span lengths of 24 m, 32 m, and 40 m, respectively.

2.2.3 Rigid-Flexible Model of VTB System

The combination of finite element software and multi-body dynamics software is used to refine simulate the vehicle-rail-bridge system to realize the data exchange between the bridge-rail model and the vehicle model by the wheel-rail contact relationship, and the conduct the dynamic analysis of the whole system. Finite element analysis mainly characterizes the motion of each part of the bridge-track system by mean of the node motion, while vehicle multi-body dynamics analysis describes the motion of each part of the vehicle in the form of modal superposition. Combined with the software of ANSYS and UM, the refined rigid-flexible coupling dynamic models of three VTB coupling systems are established and the coupling dynamic equations of (1 – 3) are solved, in which Fig. 2 shows the coupling dynamic model with a 40 m span length bridge. All the degrees of freedom at both ends of the ballastless track are

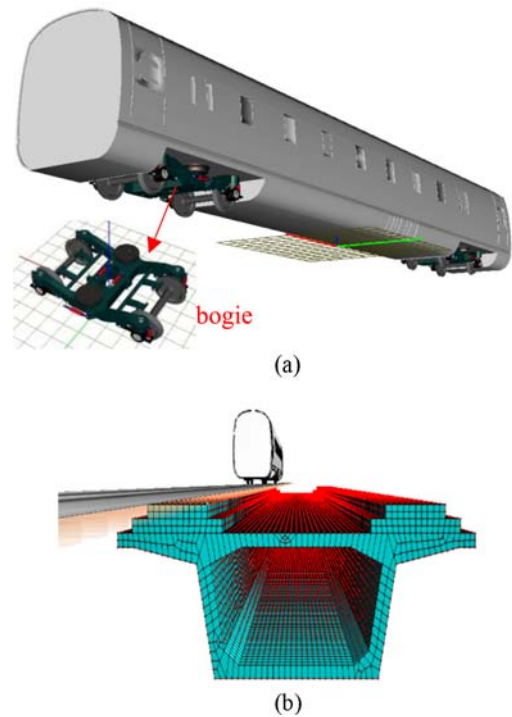


Fig. 2. Modeling the Vehicle-Track-Bridge Structure Using ANSYS and UM: (a) A Single Locomotive of the CRH380, (b) The Vehicle-Track-Bridge Coupled Dynamic Model

constrained, all the degrees of freedom at one bottom end of the box girder are constrained while only the vertical degree of freedom at the other bottom end is constrained. The straight-line length of the route is assumed to be 100 m and the initial position of the bridge distance is 30 m, as well as the simulation step is 0.0005 s. The governing equations of the VTB structures were solved by the Newmark- β method to obtain their dynamic responses.

2.3 Model Validation

2.3.1 Irregularity Spectrum Inputs

According to the China specification of TB/T 3352-2014, the track irregularity excitation is obtained from the inversion of the ballastless track irregularity in China's high-speed railway, in which the uneven length is set to 550 m, the wavelength is set to 2 – 200 m, as shown in Fig. 3. Besides, the PARK Parallel algorithm was used to solve the dynamic equations of the coupling VTB system. To simulate the wheel-rail contact geometry relationship, the LMA tread and RAIL60 rail are used for the wheel profile and steel rail, respectively. The normal force of wheel-rail is solved by Hertzian nonlinear elastic contact theory, and the creep force between wheel and rail was calculated by FASTSIM algorithm.

2.3.2 Dynamic Indicators of the Scoupled VTB System

According to the Chinese technical standards of the high-speed railway (i.e., TB 10621-2014 and TB 10761-2013 [25-27]), the dynamic indicators of the coupled VTB system are as follows when the influence of structural deformation and track deformation

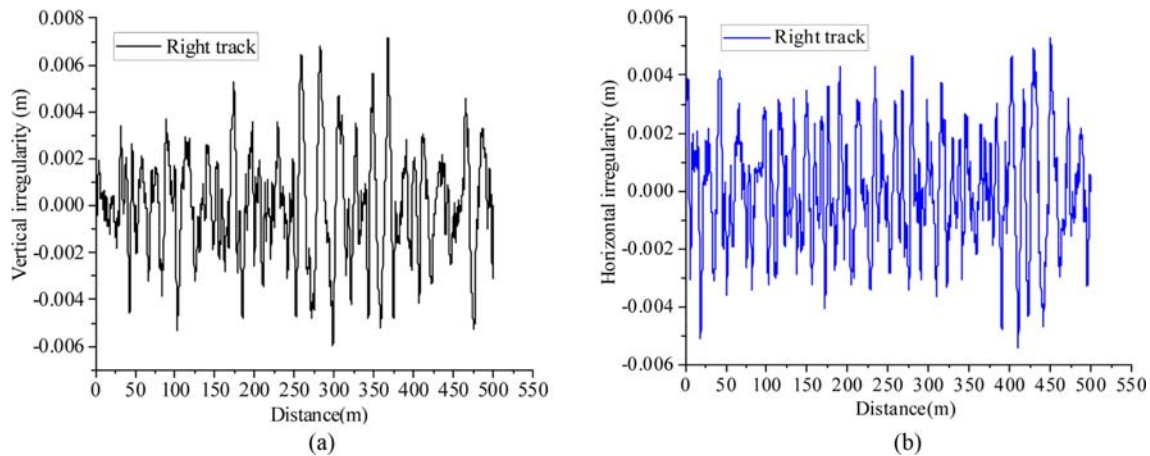


Fig. 3. The Track Irregularity Excitation: (a) Vertical, (b) Horizontal

is considered at the same time, such as, Derailment coefficient (DC), Wheel load reduction rate (WLRR), Wheel-rail contact transverse/horizontal force (H), Acceleration of train body vibration, Displacement and acceleration indicators of the ballastless track, the allowable range of lateral displacement for the bridge.

2.3.3 Rigid-Flexible Model of the Coupled VTB System

To validate the refined rigid-flexible coupling model for the VTB system, the predicted dynamic responses from the coupled VTB model were compared with the field measurement results of Zhai et al. (2013a, 2013b) which focused on investigating the dynamic responses of the 32 m long Yangcun Bridge in Beijing-Tianjin high-speed railway. CHR3 train with a speed ranging from 200 km/h to 380 km/h was used in the experimental testing, and the measured results of the 575th span of the bridge were used in this study.

2.4 Model Validation

According to the comparison of the DC, WLRR, Vertical Acceleration (VA), and Lateral Wheel-rail Contact Force (LWCF) from the 200 to 400 km/h, Fig. 4 shows that our refined coupling model results agree well with the measured results of Zhai et al. (2013a, 2013b) with the difference below 10%. Hence, the rigid-flexible coupling model could simulate the dynamic performance of the VTB system.

3. Results and Discussions

3.1 Parametric Studies

The validated vehicle-track-bridge dynamic model was used to apply various parametric studies for evaluating the coupled system under different train conditions (i.e., speed from 200 to 400 m/s with the interval of 50 m/s, and the train load from 0%, 50%, and 100% with the interval of 50%) and lengths of bridge span (i.e., 24 m, 32 m, and 40 m). The weight of bogies, wheel pair, tumbler axle-box, and full capacity for three train loading weights are 3,338, 1,869, 50, and 66,020 kg.

3.2 Results of Parametric Studies

3.2.1 Effect of Train Speeds

3.2.1.1 Dynamic Responses of the Train Model

Figure 5 illustrates that the derailment coefficient for three bridge spans initially remains unchanged when the train speed is smaller than 350 km/h, and then rapidly increases as train speed increase to 400 km/h. The increase is more obvious for a longer bridge span (i.e., 40 m). Fig. 5 shows the WLRR, acceleration and contact force (i.e., lateral and vertical) of three bridge spans gradually increase as the train speed increases, and the values of these parameters are generally large under a longer bridge span. Specifically, the value of WLRR of the 40 m span increases nonlinearly from about 0.35 to 0.82 when the speed reaches 200 to 400 km/h, and the highest increase rate of WLRR is about 75% in 250 to 350 km/h. Importantly, it should be mentioned that the WLRR of the 32 m is smaller than those of 24 m, and the value is over the limitation of 0.6 when the speed is faster than 350 km/h. Most of the lateral acceleration peak values under three bridge spans are larger than 0.6 m/s^2 , which indicates their lateral accelerations fail to meet the requirements of high-speed train design specifications. The peak values of all acceleration (i.e., lateral and vertical) under 400 km/h are still smaller than 0.9 m/s^2 , which indicates that their vertical accelerations can fulfill the specification requirements in three bridge spans. As the speed reaches 200 to 400 km/h, the vertical acceleration growth rates of 24 m, 32 m, and 40 m are about 55%, 42% and 30%, respectively. Also, the LWCF under five train speeds are much smaller than those corresponding to vertical contact forces, since the largest values of the LWCF and VWCF of the 40 m under 400 km/h are about 21 kN and 280 kN, respectively. The growth rate LWCF from 250 to 300 km/h is the largest with a growth rate of about 40% for the 24 m and 32 m spans, whereas the growth rate of vertical contact force from 350 to 400 km/h are largest with the growth rate of about 20% for the 40 m span. In summary, the dynamic performance of the train model becomes larger as the train speed increases, and the growth rate of the acceleration and

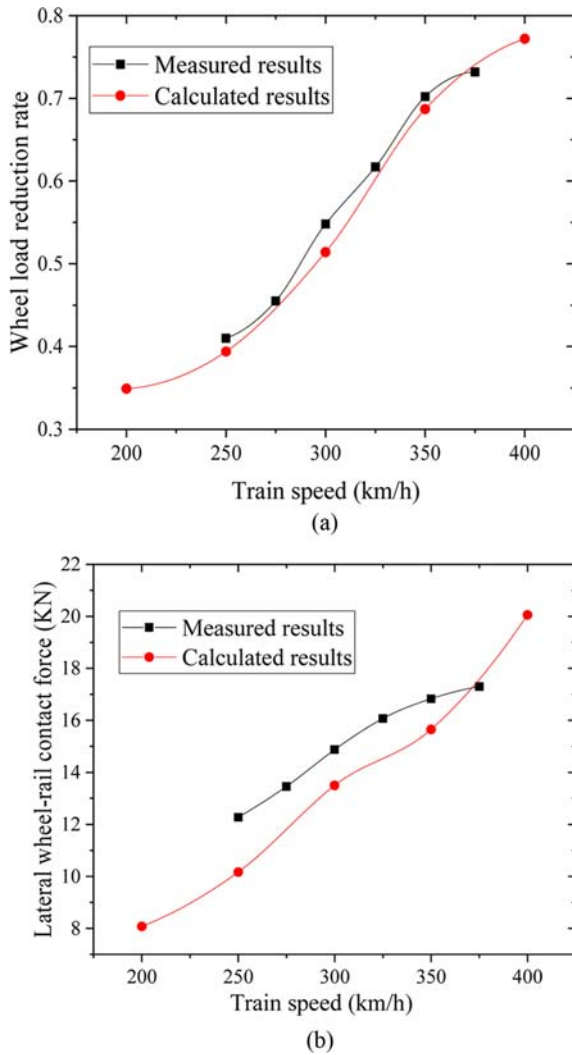


Fig. 4. The Comparison of Model Predictions and Measured Results: (a) Rate of Wheel Load Reduction, (b) Wheel-Rail Lateral Contact Force

contact force from 350 to 400 km/h is the largest.

3.2.1.2 Dynamic Response of the Track Structure

Figure 6 presents that the lateral displacement in track slab initially decreases from 200 km/h to 300 km/h, and then increases from 300 km/h to 400 km/h, which is opposite to the vertical displacement due to the longitudinal constraint in adjacent slab tracks and the buffer function of CAM between the track slab and base plate. The lateral displacement responses with the 32 m span are the largest with a displacement of 0.4 mm under the train speed of 400 km/h, whereas the vertical displacement responses are the largest with a displacement of 1.1 mm under the train speed of 300 km/h in the 40 m span bridge. Meanwhile, the accelerations (i.e., lateral and vertical) steadily increase as the train speed increases. The lateral accelerations of the track slab with the 24 m span are the largest and reach the peak value of about 0.87 m/s^2 under 400 km/h. Meanwhile, the vertical accelerations of the track slab with the 24 m span are the largest over 300 km/h

and reach the peak value of about 1.6 m/s^2 under 400 km/h. Therefore, the largest vertical displacement appear at 300 km/h for all three bridge spans. At the 400 km/h, the highest and lowest acceleration responses of the track slab occur on the 24 m and 40 m span bridge, respectively.

Figure 7 indicates that the lateral displacement of the base plate initially decreases with the train speed increase, reaches its lowest value under 300 km/h, and then increases as the train speed increase. In contrast, vertical displacement response in the base plate increases to the peak at 300 km/h and then gradually decreases as the train speed increase due to the the buffer function of CAM between the track slab and base plate. When the speed is 300 km/h, the Lateral Displacement of the base plate under the 40 m span is the largest (i.e., 0.98 mm), and the vertical displacement under the 24 m span is the largest (i.e., 0.91 mm). The acceleration (i.e., vertical and lateral) responses of the base plate generally increase with the increment of train speed and a significant increase can be seen when the speed is faster than 300 km/h. Different from the acceleration responses of the track slab, the lateral acceleration in the base plate for the 24 m span under the 400 km/h train speed is the largest (i.e., 0.9 m/s^2) and the vertical acceleration for the 40 m span is the largest (i.e., 1.5 m/s^2).

3.2.1.3 Dynamic Performances Comparison of the Bridge Structure

Figure 8. shows that the growth rate in the amplitude of the displacement (lateral and vertical) performances is relatively larger than those of the accelerations. For instance, the displacement value of the 40 m span is 0.8 mm and 1.2 mm, respectively. The displacement values decrease with the bridge span shorter. Both lateral and vertical acceleration increases with train speed and the vertical direction of the 24 m span is the maximum value (i.e., 0.66 m/s^2). It demonstrates that the dynamic performance of these three spans bridge meets the specification requirements and the 40 m span has the largest displacement.

3.2.1.4 Vibration Transmission in the Track-Bridge Structure

Figure 9 shows that the train speed leads the vertical acceleration transmission between the track slab structure and base plate structure gradually increases, and the acceleration transmission for the 24 m span is the largest, especially before 300 km/h. The vertical acceleration transmissions for the 32 m and 40 m spans are close to 1.0 under the train speed of 400 km/h. In contrast, the train speed improvement leads to the vertical acceleration transmission within the base plate structure and the box girder structure slightly decreases. Below the speed of 200 km/h, the transmission is the largest among five train speeds and the transmission of the 24 m span is larger than that of two other spans. The vertical acceleration transmission under the 400 km/h of the span of 24 m, 32 m, and 40 m is 0.47, 0.41, and 0.39, respectively. In addition, the transmission of lateral acceleration between the track slab and base plate steadily rises as the train speed increases, except for the 24 m span. For instance, as shown

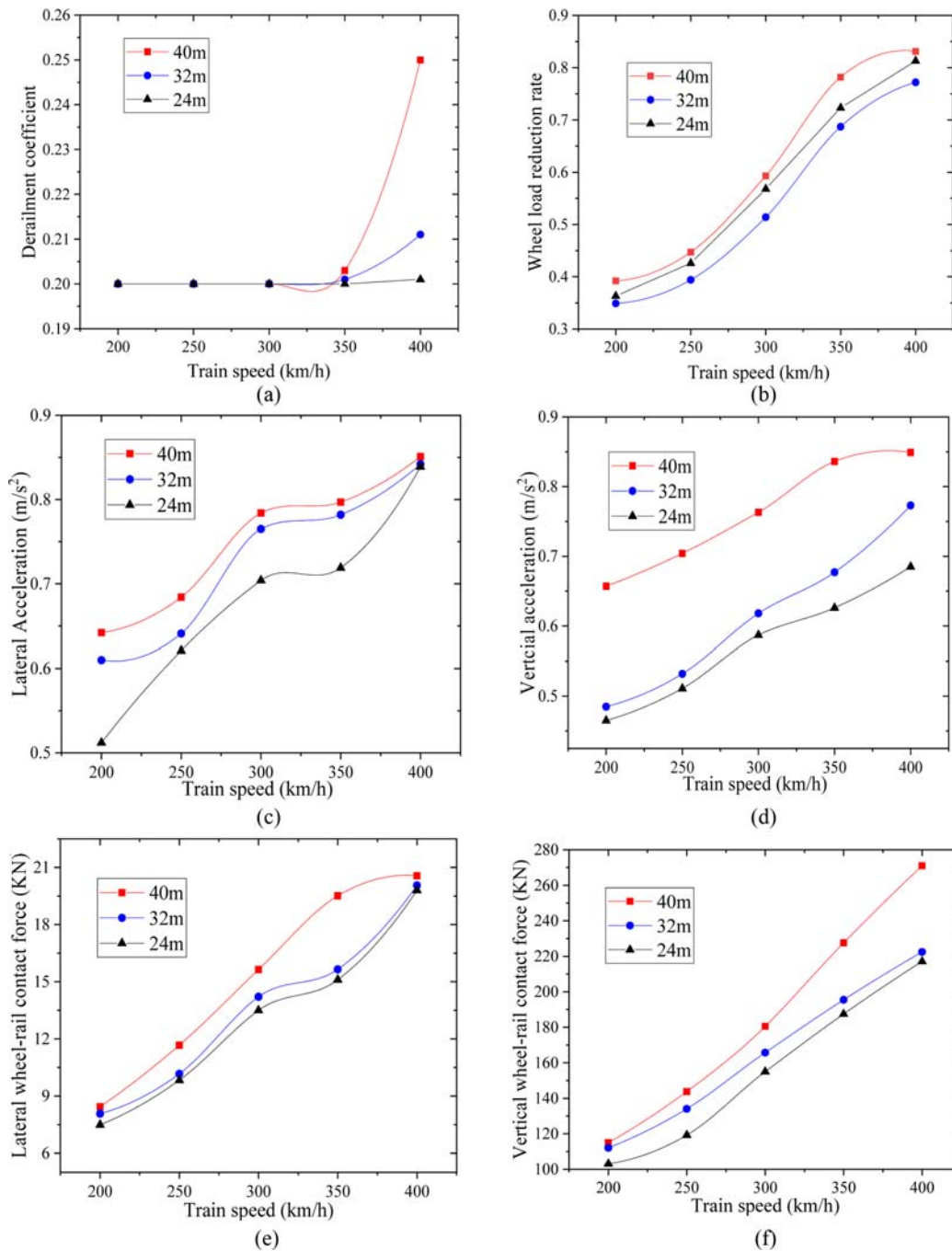


Fig. 5. Dynamic Indicators of the Train for 24 m, 32 m, 40 m Bridge Spans under Various Train Speeds: (a) DC, (b) WLRR, (c) Lateral Acceleration, (d) Vertical Acceleration, (e) Lateral Wheel-Rail Contact Force, (f) Vertical Wheel-Rail Contact Force

in Fig. 9, the lateral acceleration transmission of the 24 m, 32 m, and 40 m span in the track structure are about 0.988, 0.983, and 0.978 under the 400 km/h, respectively. The lateral acceleration transmission between the base plate structure and box girder structure of the 24 m and 32 m spans gradually decreases as the train speed increases. Importantly, the train speed improvement leads to lateral acceleration transmission of the 40 m span initially increasing and then decreasing after the 300 km/h. The largest and smallest lateral acceleration transmission of the 40 m

span is about 0.88 under the 300 km/h and about 0.53 under the 400 km/h, respectively. In conclusion, the train speed improvement leads to the increase of acceleration transmission between the track slab and base plate, while the acceleration transmission between the base plate structure and box girder structure becomes smaller. In addition, the vertical acceleration transmission in the track structure under 400 km/h is close to 1 and all the lateral acceleration transmissions in the track structure for the 24 m span are relatively large.

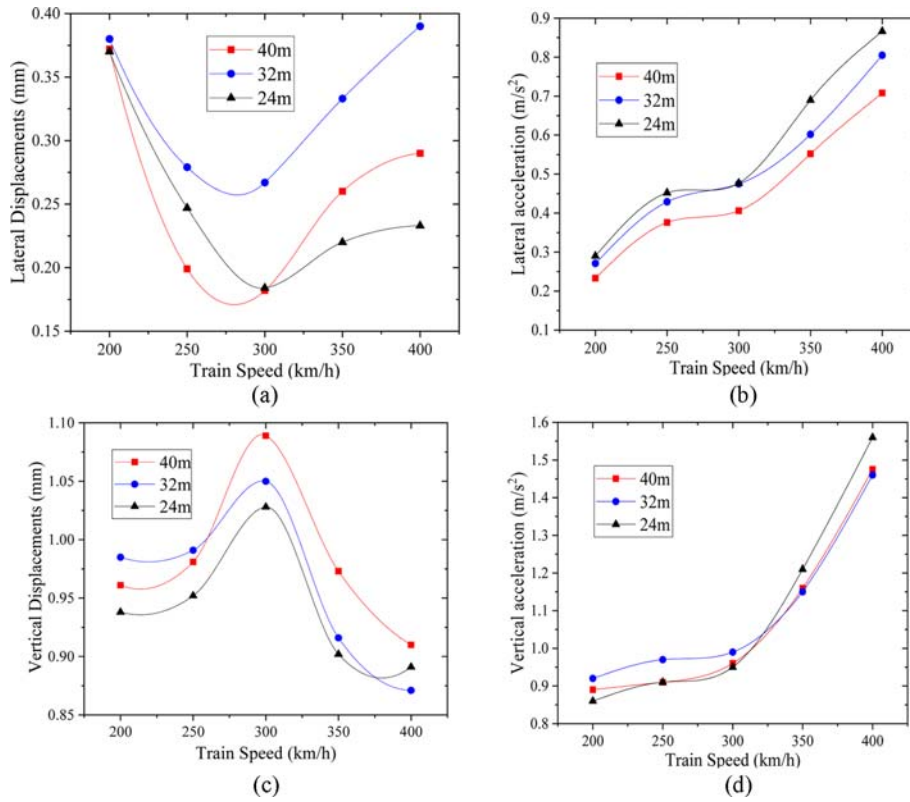


Fig. 6. Track Slab Dynamic Performance under the Combination of Different Bridge Spans and Train Speeds, (a) Lateral Displacement Response, (b) Lateral Acceleration Response, (c) Vertical Displacement Response, (d) Vertical Acceleration Response

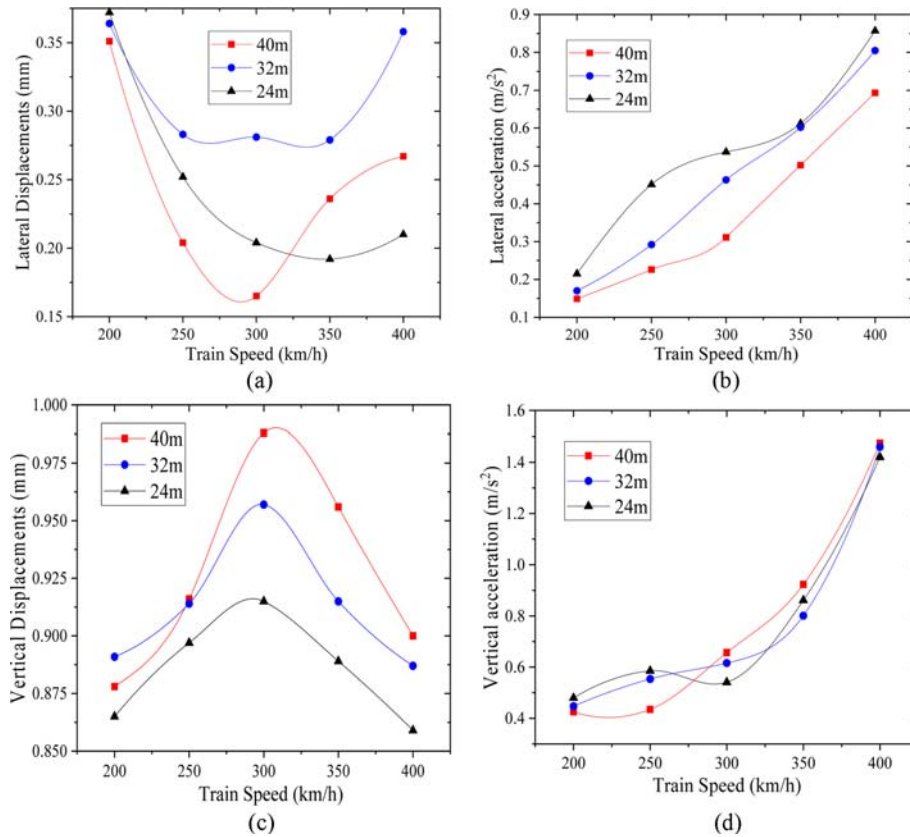


Fig. 7. Dynamic Responses of the Base Plate under the Combination of Different Bridge Spans and Train Speeds: (a) Lateral Displacement Response, (b) Lateral Acceleration Response, (c) Vertical Displacement Response, (d) Vertical Acceleration Response

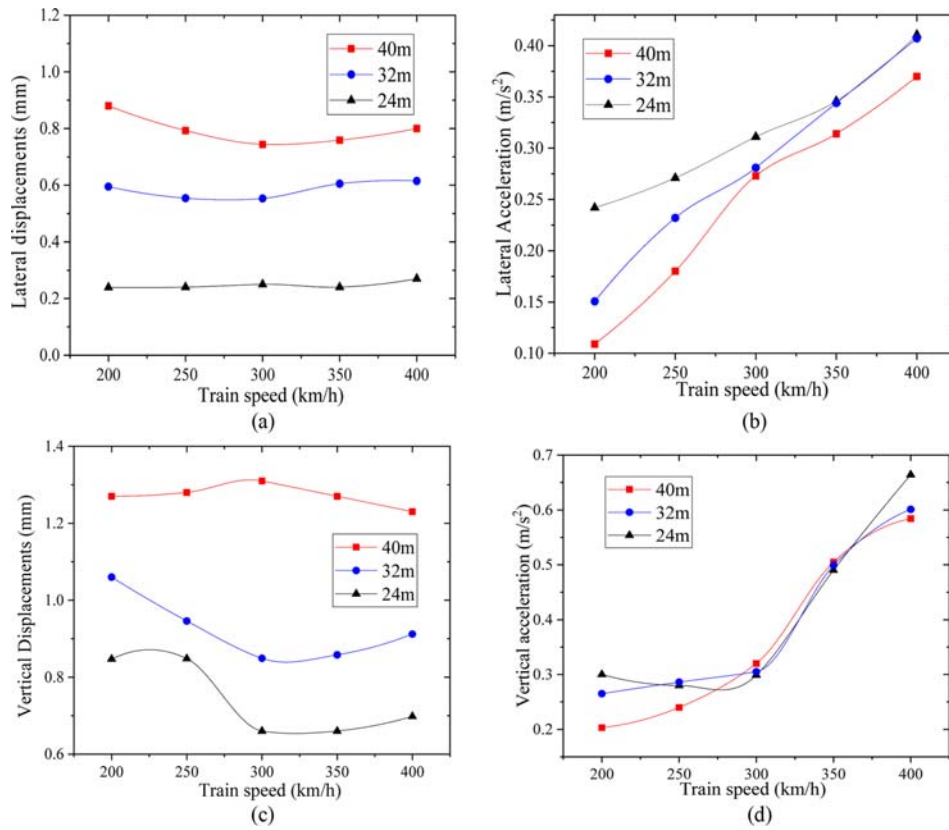


Fig. 8. Dynamic Responses of the Bridge under the Combination of Different Bridge Spans and Train Speeds, (a) Lateral Displacement Response, (b) Vertical Displacement Response

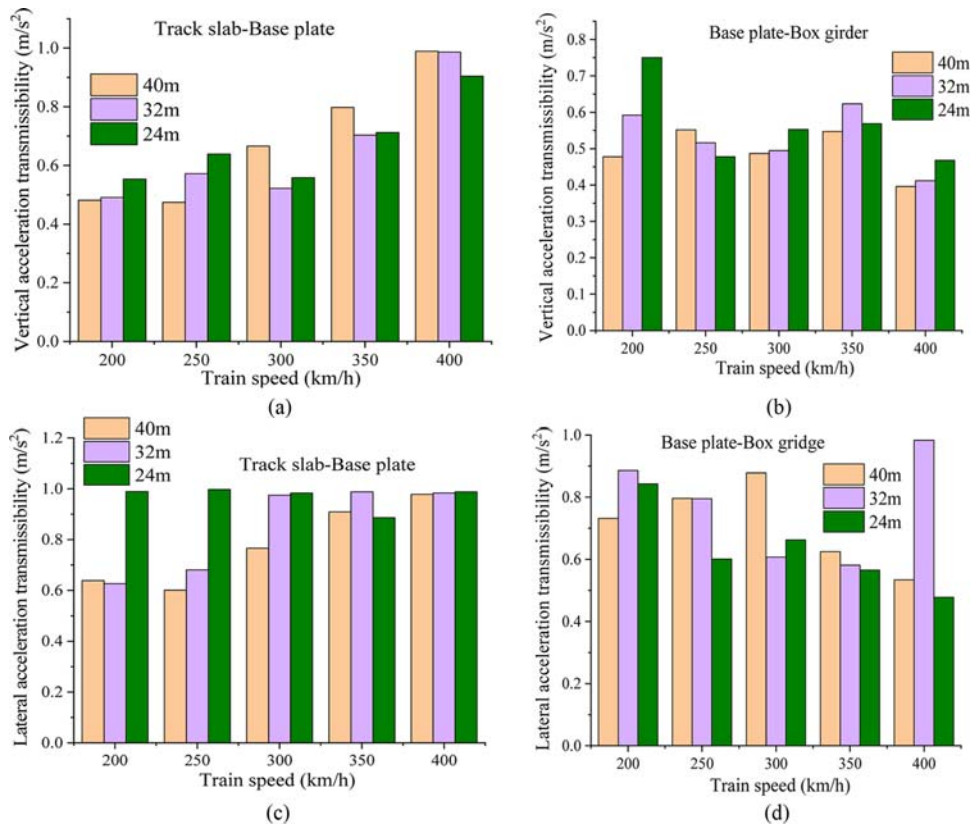


Fig. 9. Acceleration Transmission between the Components of the Track-Bridge Structure, (a-b) Vertical Transmission between Track Slab-Base Plate and Base Plate-Box Girder, (c-d) Lateral Transmission between Track Slab-Base plate and Base Plate-Box Girder

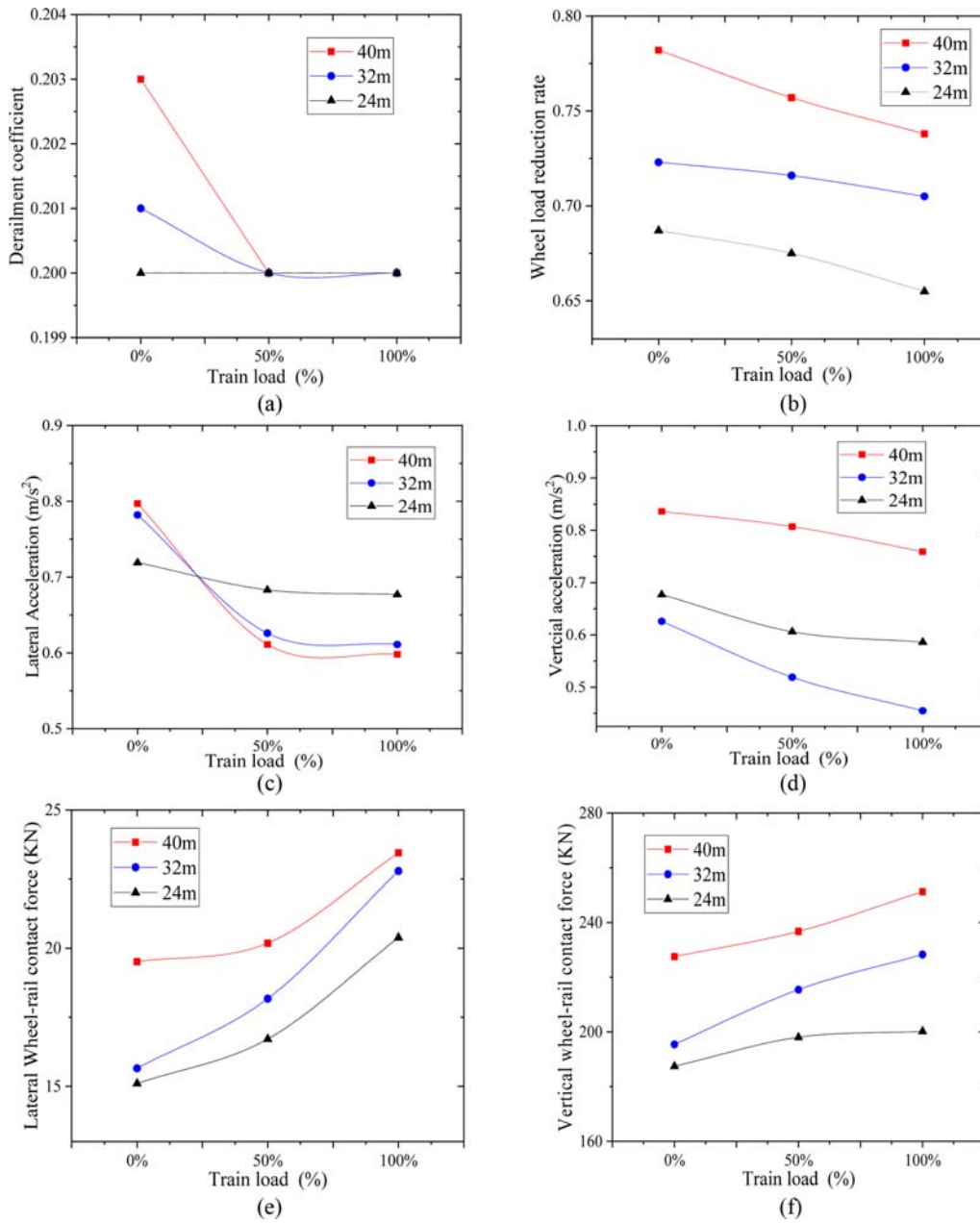


Fig. 10. Dynamic Indicators of the Train for Three Bridge Spans under Various Levels of Train Loads: (a) DC, (b) WLRR, (c) LA, (d) VA, (e) LWCF, (f) VWCF

3.2.2 Effect of bridge spans

3.2.2.1 Dynamic Responses Comparison of Train Model

Figure 10 shows the dynamic indicators of the train for 24 m, 32 m, and 40 m bridge spans under various train loads (100% capacity = 66,020 kg). It shows that the DC, WLRR, and Acceleration decrease with the increase of the train load, whereas the WRCF increases. The derailment coefficients under three levels of train load maintain about 0.2 for all three spans. It should be noted that the WLRR of the 40 m span is larger than those of the other two spans, and the WLRR of the 40 m span with the 100% train load

capacity is 0.74. Under 100% capacity, the lateral acceleration of the 24 m span and vertical acceleration of the 40 m span is the largest (i.e., about 0.68 m/s² and 0.75 m/s²). Furthermore, both the lateral and vertical wheel-rail contact forces of the 40 m span are also larger than those of the other two spans with their maximum values of 23 kN and 250 kN, under 100% capacity. The contact forces of the train become larger with the increase of bridge span, which is different from the effects of the train’s acceleration due to the significant increase in the weight of the train itself. Notably, the vertical wheel-rail contact forces of the 40 m span are close to the allowable limit values.

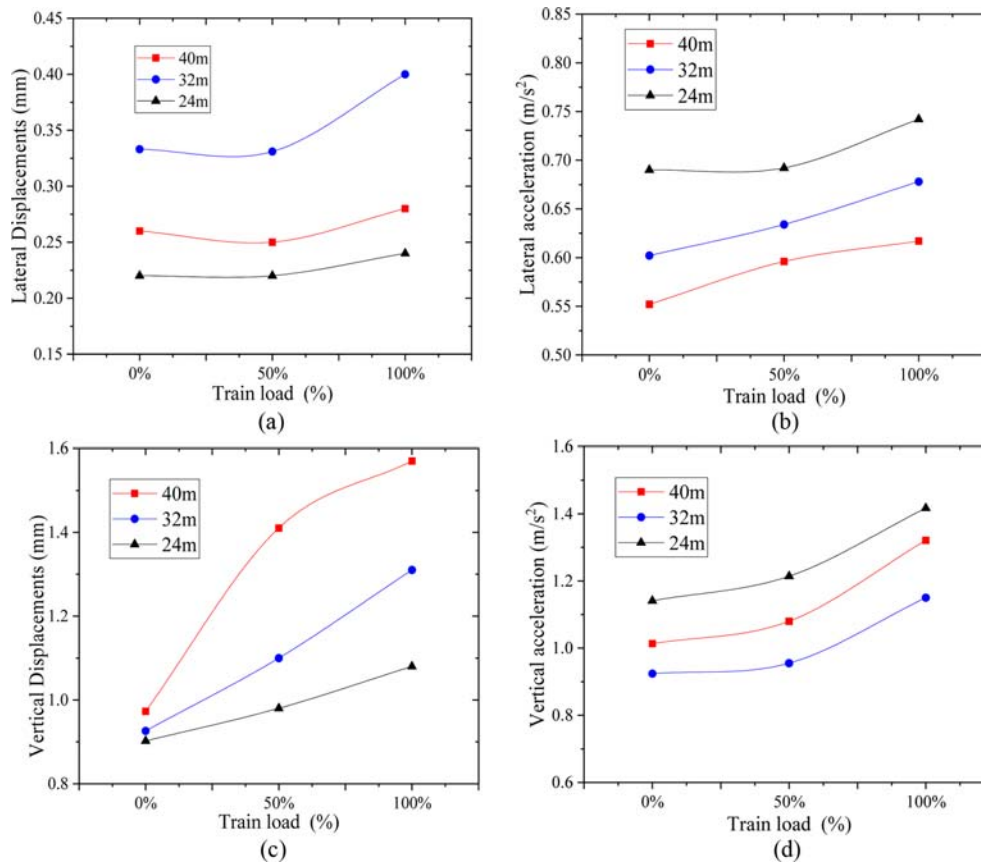


Fig. 11. Dynamic Performances for Three Bridge Spans under Various Levels of Train Loads: (a) Lateral Displacement Response, (b) Lateral Acceleration Response, (c) Vertical Displacement Response, (d) Vertical Acceleration Response

3.2.2.2 Dynamic Responses of Track Structure

Figure 11 shows that both the lateral displacement and acceleration in the track slab increase with the increase of train load. In particular, the lateral displacement of the 32 m span are much larger than those of two other spans, while the lateral accelerations of the 24 m span are the largest among the three spans. The growth rate of the lateral displacement and acceleration for the 32 m span under the full capacity of the train load is 23.3%. In the track slab, the vertical displacement also increases as the train load increases. The vertical displacement responses of the 40 m span are significantly larger than those of the other two spans, and their maximum value is 1.0 mm, 1.4 mm, and 1.6 mm under the 0%, 50%, and 100% train load, respectively. Vertical acceleration's maximum value in the track slab of the 24 m span is also the largest. In the track slab, the displacement and acceleration response meets the specification requirements under different levels of train load.

Figure 12 shows that both the displacement and acceleration performances of the base plate increase as the level of train load increases. The lateral displacement of the 32 m span is much larger than that of the other two spans with maximum values of 0.275 mm, 0.3 mm, and 0.33 mm under the 0%, 50%, and 100% train load, respectively. The maximum values of the vertical displacement for the 40 m span are 1.0 mm, 1.4 mm, and 1.55 mm under the 0%, 50%, and 100% train load, respectively. The

vertical direction (i.e., displacement and acceleration) of the 40 m span in the base plate is significantly greater than those of the two other spans. Moreover, the maximum values of vertical acceleration for the 40 m span are $0.9 m/s^2$, $1.1 m/s^2$, and $1.2 m/s^2$ under the 0%, 50% and 100% train load, respectively. Among these three spans, the maximum vertical acceleration in the base plate of the 40m span is the largest, with an increase rate of 10.5% and 18.6%, respectively. As a result, the lateral and vertical acceleration in the base plate meets the specification requirements under different train loads.

3.2.2.3 Dynamic Responses of Three Bridge Structures

The displacement and acceleration responses of the three box girders increase in lateral and vertical directions as the train load increases, as compared in Fig. 13. Both the lateral and vertical displacement responses of the 40 m span are much larger than that of the two other spans. For example, the maximum lateral displacement and vertical displacement under a 100% train load measure approximately 1 mm and 1.7 mm, respectively. The increase rate of the lateral and vertical displacement of the 40 m span is 32.8% and 30.8%, respectively. Besides, the lateral acceleration of the 24 m span is the largest with a maximum value of $0.55 m/s^2$ under the 100% train load, whereas the vertical acceleration of the 40 m span is the largest with the $0.65 m/s^2$

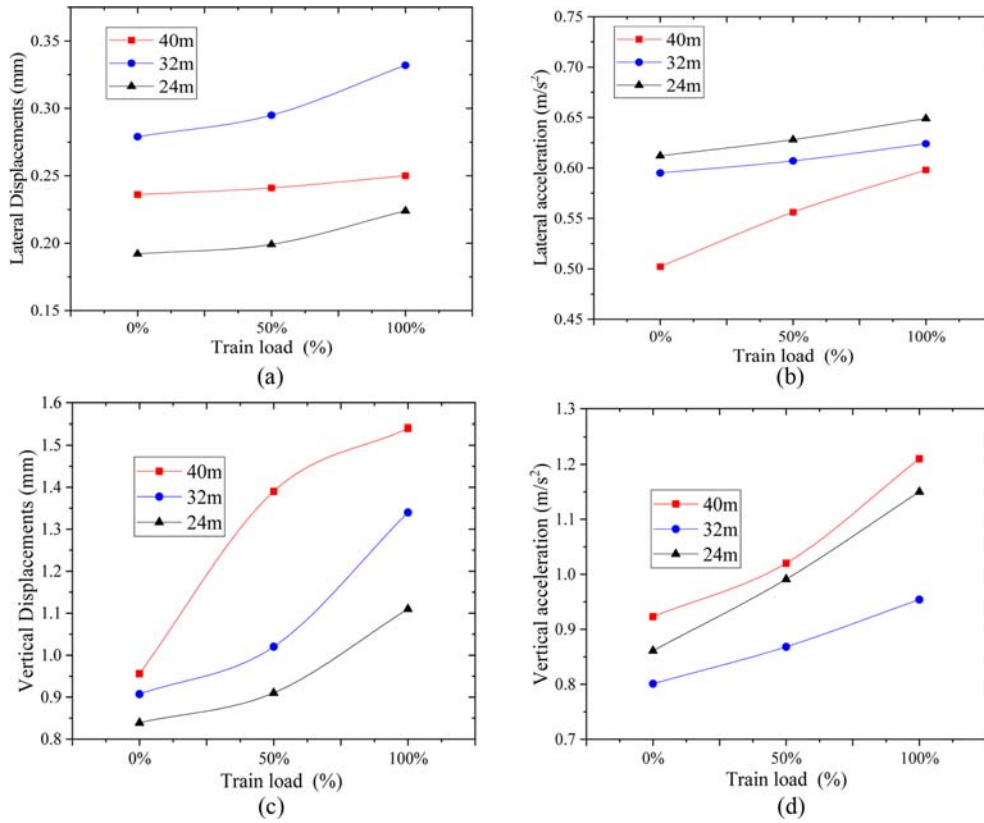


Fig. 12. Dynamic Responses of the Base Plate for Three Bridge Spans under Various Levels of Train Loads: (a) Lateral Displacement Response, (b) Lateral Acceleration Response, (c) Vertical Displacement Response, (d) Vertical Acceleration Response

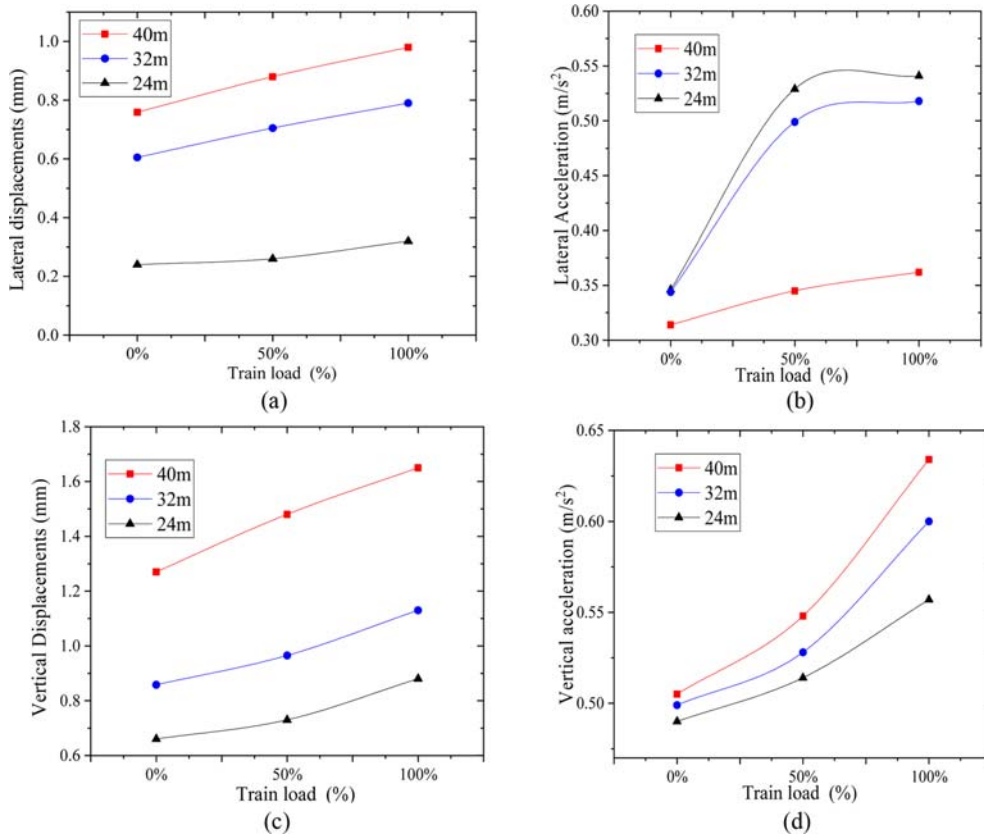


Fig. 13. Dynamic Responses of Three Bridge Span Structures under Various Levels of Train Loads: (a) Lateral Displacement Response, (b) Lateral Acceleration Response, (c) Vertical Displacement Response, (d) Vertical Acceleration Response

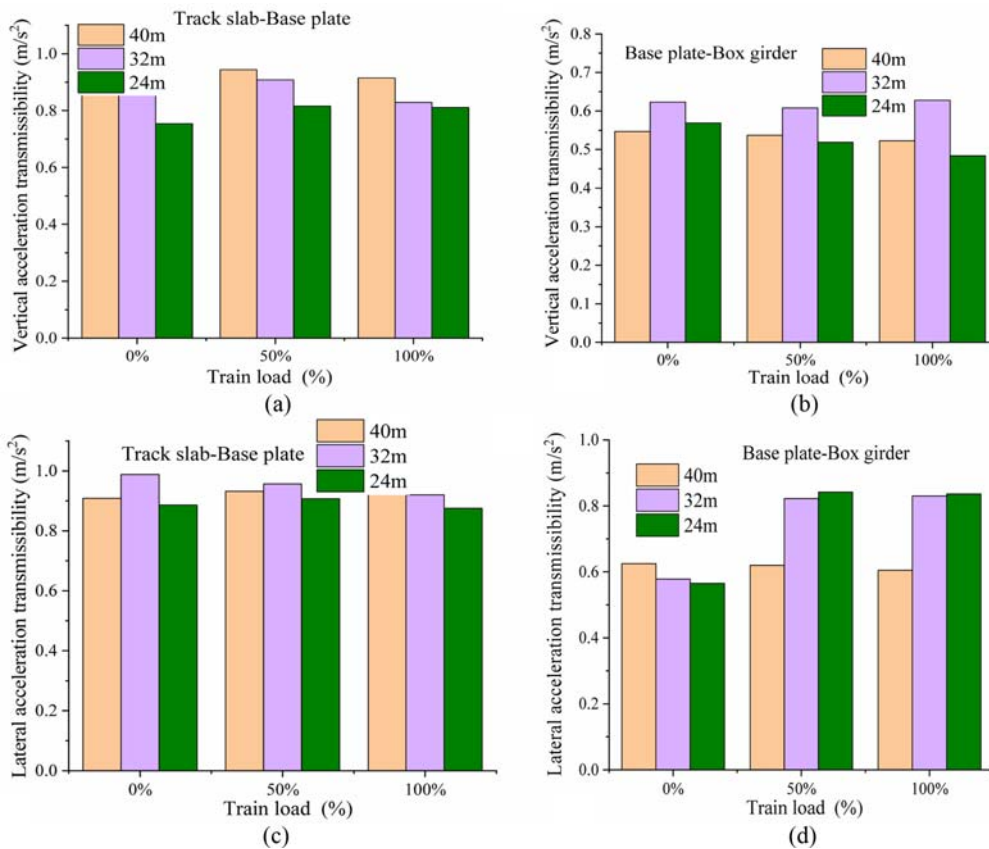


Fig. 14. Acceleration Transmission between the Components of Three Bridge Spans under Various Levels of Train Loads: (a) Lateral Displacement Response, (b) Lateral Acceleration Response, (c) Vertical Displacement Response, (d) Vertical Acceleration Response

under the 100% train load. The vertical acceleration increases by approximately 26%, 20%, and 16% for the 24 m, 32 m, and 40 m spans, respectively, as the train load rises from 0% to 100%. The effect of the train load on the vertical direction (i.e., displacement and acceleration) of the bridges is particularly pronounced, especially for the 40 m span.

3.2.2.4 Vibration Transmission between Track-Bridges Structure

Figure 14 shows that the vertical acceleration transmission between the track slab and base plate gradually increases with the train load increases, which is opposite to the vertical acceleration transmission between the base plate and box girder due to the buffer function of CAM between the track slab and base plate. Vertical acceleration transmission in the track structure of the 40 m and 24 m span is the largest and smallest among the three spans, respectively. However, the vertical acceleration transmission between the base plate and box girder of the 32 m and 24 m span is the largest and smallest among the three spans, respectively. It should be noted that the vertical acceleration transmission in the track structure under the 100% train load is close to 0.9, which indicates that the heavier train load is unfavorable to the vertical acceleration transmission in the track structure. As the train load increases, the lateral acceleration transmission between the track slab and base plate gradually increases. Notably, the increment is

the smallest for the 32 m span. In the case of both the 32 m and 24 m spans, the acceleration transmission between the base plate and box girder increases with the growing train load. More specifically, the lateral acceleration transmissions of the 32 m and 24 m in the track structure are 0.92 and 0.875, respectively, and their lateral acceleration transmission in the track-bridge structure is close to 0.83. The transmission of both lateral and vertical acceleration in the 40 m section of the track-bridge structure is notably substantial. As a result, the acceleration transmission within the multi-layer components of the track-bridge structure exhibits a strong sensitivity to the train load, particularly for a full 100% train load.

4. Discussion

Based on the combination of ANSYS and Universal Mechanism software, the refined rigid-flexible coupling models of vehicle-CRTS II track-bridge with three span lengths was developed and verified in this study. The comprehensive dynamic performance of the train, track slab, base plate and box girder with three typical spans (24 m, 32 m, and 40 m) are analyzed under various train speeds and weights, respectively. The refined rigid-flexible coupled model could effectively simulate the dynamic performance of the vehicle-ballastless track-bridge with three bridge span lengths by compared with the measured results of 32 m span. As

the train speed increases from 200 km/h to 400 km/h, the dynamic indicators of the train, and the accelerations of track slab, base plate and box girder gradually increase, as well as the growth rates of these dynamic responses after the 300 km/h obviously become larger. As the train loads increase from 0% to 100% loading rate, the displacement and acceleration of the track and bridge structure gradually increase, while the wheel-rail contact force and contact force of the train in later and vertical direction gradually decrease. Most of the dynamic responses of the track-bridge structure with 40 m span are larger than those of the 24 m and 32 m. With the increase of the train speed and weight, the vertical acceleration transmission between the track slab and base plate gradually becomes larger, while the vertical acceleration transmission in the track-bridge structure becomes smaller. The displacement and acceleration responses of the current track-bridge structure meet the specification requirements under updated 400 km/h train speed and 100% train.

5. Conclusions

This study investigated the vibration transmission of three track-bridge structures under different train loads and bridge spans through the validated rigid-flexible model for the coupling vehicle-longitudinal slab track-bridge system. The following are some major conclusions:

1. The derailment coefficient initially remains unchanged, and then significantly increases when the train speed is over 350 km/h. Their growth rate is more obvious with the increase in the bridge span. In addition, the WLRR, acceleration, and contract force gradually rise with increasing train speed, and the magnitude of these parameters increases as the bridge span increases.
2. Track slab lateral displacement initially decreases from 200 km/h to 300 km/h, and then increases when the train speed is over 300 km/h. The largest vertical displacement of the rack slab happens when the train speed is 300 km/h.
3. Base plate lateral displacement initially decreases with increasing train speed, reaching its lowest value at speeds up to 300 km/h, after which it increases with further speed increments. Conversely, the vertical displacement response of the base plate initially increases, reaching its peak at 300 km/h, and then gradually decreases as the train speed continues to increase.
4. Vertical acceleration transmission between the track slab and base plate gradually increases with increasing train speed. Among the five train speeds, the transmission at 200 km/h is the largest, and the transmission for the 24 m span is greater than that for the other two spans.



It should be pointed out that the vibration transmission and dynamic responses of the coupling vehicle-longitudinal slab track-bridge system are analyzed based on the Code for Design of China High Speed Railway. Nevertheless, the influence of different types of ballastless tracks and track irregularity excitations on the dynamic characteristics of the coupling vehicle-track-

bridge system. The thermo-mechanical effect of the coupling vehicle-longitudinal slab track-bridge system under the coupling temperature and train loads is the next work in future (Zhou et al., 2023).

Acknowledgments

The authors gratefully acknowledge support from the Project of Science and Technology Research and Development Program of China State Railway Group Co., Ltd. (K2022G038), National Natural Science Foundation of China (No.52278311), the Guangdong Natural Science Foundation (No.2023A1515030148), the Shenzhen Science and Technology Program (Nos. GJHZ20220913143006012 and JCYJ20220531101609020), the State Key Laboratory of Mountain Bridge and Tunnel Engineering (No. SKLBT-ZD2101), State Key Laboratory of Performance Monitoring and Protecting of Rail Transit Infrastructure, East China Jiaotong University (No. HJGZ2023105), Guizhou University Doctoral Fund [2022] 68, Guizhou Provincial Basic Research Program (Natural Science) (No. QianKeHeJiChu-ZK [2024] YiBan 070), MOE Key Laboratory of High-Speed, RailwayEngineering, Southwest Jiaotong University: 2021 and 2022 Open Fund, National Key Laboratory of Green and Long-Life Road Engineering in Extreme Environment (Shenzhen University).

ORCID

Rui Zhou  <https://orcid.org/0000-0002-9167-403X>
Hanlin Liu  <https://orcid.org/0000-0002-2673-5289>

References

- Chen Z (2020) Evaluation of longitudinal connected track under combined action of running train and long-term bridge deformation. *Journal of Vibration and Control* 26(7-8):599-609, DOI: 10.1177/1077546319889855
- Chen Z, Zhai W, Cai C, Sun Y (2015) Safety threshold of high-speed railway pier settlement based on train-track-bridge dynamic interaction. *Science China Technological Sciences* 58:202-10, DOI: 10.1007/s11431-014-5692-0
- Chen R, Zhao X, Wang Z, Jiang H, Bian X (2013) Experimental study on dynamic load magnification factor for ballastless track-subgrade of high-speed railway. *Journal of Rock Mechanics and Geotechnical Engineering* 5(4):306-11, DOI: 10.1016/j.jrmge.2013.04.004
- Code for Design of High Speed Railway. State Railway Administration of China (2014) State Railway Administration of China. TB 10621-2014
- Gautier PE (2015) Slab track: Review of existing systems and optimization potentials including very high speed. *Construction and Building Materials* 92:9-15, DOI: 10.1016/j.conbuildmat.2015.03.102
- Gong W, Zhu Z, Wang K, Yang W, Bai Y, Ren J (2021) A real-time co-simulation solution for train-track-bridge interaction. *Journal of Vibration and Control* 27(13-14):1606-16, DOI: 10.1177/1077546320946631
- Jeon BG, Kim NS, Kim SI (2016) Estimation of the vibration serviceability

- deflection limit of a high-speed railway bridge considering the bridge-train interaction and travel speed. *KSCE Journal of Civil Engineering* 20:747-61, DOI: [10.1007/s12205-015-0565-z](https://doi.org/10.1007/s12205-015-0565-z)
- Li XZ, Lei HJ, Zhu Y (2013) Analysis of Rayleigh damping parameters in a dynamic system of vehicle-track-bridge. *Journal of Vibration and Shock* 32(21):52-57
- Matias SR, Ferreira PA (2020) Railway slab track systems: review and research potentials. *Structure and Infrastructure Engineering* 16(12): 1635-53, DOI: [10.1080/15732479.2020.1719167](https://doi.org/10.1080/15732479.2020.1719167)
- Montenegro PA, Carvalho H, Ribeiro D, Calçada R, Tokunaga M, Tanabe M, Zhai WM (2021) Assessment of train running safety on bridges: A literature review. *Engineering Structures* 241:112425, DOI: [10.1016/j.engstruct.2021.112425](https://doi.org/10.1016/j.engstruct.2021.112425)
- PSD of ballastless track Irregularities of high-speed railway (2014) State Railway Administration of China. 2014, TB/T 3352-2014
- Ren J, Chen Y, Sun Z, Zhang Y (2023) A vehicle-bridge interaction vibration model considering bridge deck pavement. *Journal of Low Frequency Noise, Vibration and Active Control* 42(1):146-72, DOI: [10.1177/14613484221122736](https://doi.org/10.1177/14613484221122736)
- Technical regulations for dynamic acceptance for high-speed railways construction (2013) Ministry of Railways of China. TB 10761-2013
- Xia CY, Lei JQ, Zhang N (2012) Coupled vibration analysis for train and simply-supported bridge system subjected to floating-ice collision. *Zhendong yu Chongji (Journal of Vibration and Shock)* 31(13):154-8
- Xiang P, Wei M, Sun M, Li Q, Jiang L, Liu X, Ren J (2021) Creep effect on the dynamic response of train-track-continuous bridge system. *International Journal of Structural Stability and Dynamics* 21(10):2150139, DOI: [10.1142/S021945542150139X](https://doi.org/10.1142/S021945542150139X)
- Yan B, Dai GL, Hu N (2015) Recent development of design and construction of short span high-speed railway bridges in China. *Engineering Structures* 100:707-17, DOI: [10.1016/j.engstruct.2015.06.050](https://doi.org/10.1016/j.engstruct.2015.06.050)
- Yang J, Song Y, Lu X, Duan F, Liu Z, Chen K (2021) Validation and analysis on numerical response of super-high-speed railway pantograph-catenary interaction based on experimental test. *Shock and Vibration* 2021:1-3, DOI: [10.1155/2021/9922404](https://doi.org/10.1155/2021/9922404)
- Zhai WM (2020) Vehicle-track coupled dynamics theory and applications. Singapore: Springer; 2020
- Zhai WM, Cai CB (2002) Train/track/bridge dynamic interactions: Simulation and applications. *Vehicle System Dynamics* 37(sup1): 653-65, DOI: [10.1080/00423114.2002.11666270](https://doi.org/10.1080/00423114.2002.11666270)
- Zhai W, Liu P, Lin J, Wang K (2015a) Experimental investigation on vibration behaviour of a CRH train at speed of 350 km/h. *International Journal of Rail Transportation* 3(1):1-6, DOI: [10.1080/23248378.2014.992819](https://doi.org/10.1080/23248378.2014.992819)
- Zhai W, Wei K, Song X, Shao M (2015b) Experimental investigation into ground vibrations induced by very high speed trains on a non-ballasted track. *Soil Dynamics and Earthquake Engineering* 72:24-36, DOI: [10.1016/j.soildyn.2015.02.002](https://doi.org/10.1016/j.soildyn.2015.02.002)
- Zhai W, Wang S, Zhang N, Gao M, Xia H, Cai C, Zhao C (2013b) High-speed train-track-bridge dynamic interactions-Part II: Experimental validation and engineering application. *International Journal of Rail Transportation* 1(1-2):25-41, DOI: [10.1080/23248378.2013.791497](https://doi.org/10.1080/23248378.2013.791497)
- Zhai W, Xia H, Cai C, Gao M, Li X, Guo X, Zhang N, Wang K (2013a) High-speed train-track-bridge dynamic interactions-Part I: Theoretical model and numerical simulation. *International Journal of Rail Transportation* 1(1-2):3-24, DOI: [10.1080/23248378.2013.791498](https://doi.org/10.1080/23248378.2013.791498)
- Zhang X, Shan Y, Yang X (2017) Effect of bridge-pier differential settlement on the dynamic response of a high-speed railway train-track-bridge system. *Mathematical Problems in Engineering*, 2017, DOI: [10.1155/2017/8960628](https://doi.org/10.1155/2017/8960628)
- Zheng Z, Liu P, Liu L, Yu Z, Zhu W, He S (2022) cooperative work of CRTS II Slab Ballastless Track-32 m Simply Supported Girder under Pier Settlement. *KSCE Journal of Civil Engineering* 26(2):781-94, DOI: [10.1007/s12205-021-0413-2](https://doi.org/10.1007/s12205-021-0413-2)
- Zhou R, Yue H, Du Y, Yao G, Liu W, Ren W (2023) Experimental and numerical study on interfacial thermal behaviour of CRTS II slab track under continuous high temperatures. *Engineering Structures* 284:115964, DOI: [10.1016/j.engstruct.2023.115964](https://doi.org/10.1016/j.engstruct.2023.115964)
- Zhou R, Zhu X, Huang J, Zhou H, Liu H, Ma C, Zhang L (2022) Structural damage analysis of CRTS II slab track with various interface models under temperature combinations. *Engineering Failure Analysis* 134:106029, DOI: [10.1016/j.engfailanal.2022.106029](https://doi.org/10.1016/j.engfailanal.2022.106029)
- Zhou LY, Zhao L, Mahunon AD, Zhang YY, Li HY, Zou LF, Yuan YH (2021) Experimental study on stiffness degradation of Crts II ballastless track-bridge structural system under fatigue train load. *Construction and Building Materials* 283:122794, DOI: [10.1016/j.conbuildmat.2021.122794](https://doi.org/10.1016/j.conbuildmat.2021.122794)
- Zhu D, Yu B, Wang D, Zhang Y (2024) Fusion of finite element and machine learning methods to predict rock shear strength parameters. *Journal of Geophysics and Engineering*, gxae064, DOI: [10.1093/jge/gxae064](https://doi.org/10.1093/jge/gxae064)